Geophysical Research Letters

RESEARCH LETTER
10.1029/2019GL083397

Magnetic Reconnection in a Quasi-Parallel Shock: Two-Dimensional Local Particle-in-Cell Simulation

N. Bessho[1,2], L.-J. Chen[2], S. Wang[1,2], M. Hesse[3], and L. B. Wilson III[2]

[1]Department of Astronomy, University of Maryland, College Park, MD, USA, [2]Heliophysics Science Division, NASA Goddard Space Flight Center, Greenbelt, MD, USA, [3]Birkeland Centre for Space Science, University of Bergen, Bergen, Norway

Key Points:
- In a quasi-parallel shock, guide field reconnection occurs in the shock transition and downstream regions
- In electron-scale islands, only electron jets exist in reconnection, producing a Hall magnetic field pattern
- In ion-scale islands, both ions and electrons are involved and energized in reconnection

Correspondence to:
N. Bessho,
naoki.bessho@nasa.gov

Citation:
Bessho, N., Chen, L.-J., Wang, S., Hesse, M., & Wilson, L. B., III (2019). Magnetic reconnection in a quasi-parallel shock: Two-dimensional local particle-in-cell simulation. *Geophysical Research Letters*, *46*, 9352–9361. https://doi.org/10.1029/2019GL083397

Received 18 APR 2019
Accepted 24 JUL 2019
Accepted article online 29 JUL 2019
Published online 21 AUG 2019

Abstract Magnetic reconnection in a quasi-parallel bow shock is investigated with two-dimensional local particle-in-cell simulations. In the shock transition and downstream regions, large amplitude magnetic fluctuations exist, and abundant current sheets form. In some current sheets, reconnection occurs, and ion-scale and electron-scale magnetic islands are generated. In electron-scale island regions, only electron outflow jets are observed, producing a quadrupolar out-of-plane magnetic field pattern, while in ion-scale islands, both ions and electrons are involved and energized in reconnection. Normalized reconnection rates are obtained to be between around 0.1 to 0.2, and particle acceleration signatures are seen in distribution functions.

Plain Language Summary In the Earth's bow shock, instabilities generate winding magnetic field lines and turbulence in the shock transition region, location where magnetic field, density, and temperature rapidly increase and the bulk flow speed rapidly decreases into the downstream. Many current sheets exist in these regions, provoking magnetic reconnection to occur, which has been observed by space observations. We investigate a quasi-parallel shock (i.e., where the shock normal angle is less than 45°) by means of two-dimensional, fully kinetic (both electrons and ions are particles) simulation. Plasma parameters are defined as relevant to the Earth's bow shock. In a simulation where the shock angle is 25°, many ion-scale and electron-scale magnetic islands are generated due to magnetic reconnection. In electron-scale small island regions, only electron jets are generated in reconnection, and no ion jets exist. A quadrupolar magnetic field pattern forms due to the electron jets, and fast reconnection rates are observed. In ion-scale magnetic island regions, both ions and electrons are involved in fast reconnection. Accelerated particles due to magnetic reconnection are found in particle distribution functions, and reconnection in shock may be a viable injection mechanism for energetic particle generation through shock acceleration.

1. Introduction

In the Earth's quasi-parallel bow shock, where the shock angle is less than 45°, plasma becomes turbulent owing to instabilities excited between incident and reflected particles (Wu, 1982; Scholer, 1993; Scholer et al., 1997; Burgess et al., 2012, Burgess & Scholer, 2013, Wilson, 2016). In such turbulence, multiple current sheets can exist in both the shock transition region (foreshock and ramp) and the downstream region.

Recent space observations by Cluster and Magnetospheric Multiscale (MMS) revealed magnetic reconnection in those current sheets. Based on Cluster data, Retinò et al. (2007) observed many current sheets in the magnetosheath (shock downstream region) and reported reconnection. Yordanova et al. (2016) and Vörös et al. (2017) demonstrated signatures of ion and electron diffusion regions in magnetosheath current sheets observed by MMS. Based on MMS data, Phan et al. (2018) showed electron-scale current sheets exhibiting reconnection in the magnetosheath, where only electron but no ion jets were detected, indicating that ions cannot respond to the small-scale structures, and only electrons are involved in reconnection.

The shock transition region is also a region with high turbulence, where recent MMS observations revealed many current sheets and reconnection regions. Wang et al. (2019) investigated a shock transition with quasi-perpendicular upstream conditions and found reconnecting current sheets. The electromagnetic signatures of Hall fields were observed in the current sheets. In one event, an ion-scale sheet showed only electron jets, while in another current sheet whose thickness is several ion skin depths, both electron and

ion jets were observed. Gingell et al. (2019) studied two quasi-parallel shocks and showed reconnecting current sheets with only electron outflow jets in the transition region.

Despite the importance of investigating reconnection in shock turbulence, there have been only a few numerical studies by kinetic simulations. Karimabadi et al. (2014) demonstrated by both hybrid simulations and fully kinetic simulations that reconnection occurs in turbulence in the Earth's magnetosheath. Matsumoto et al. (2015) and Bohdan et al. (2017) studied high Alfvén Mach number (M_A~30 to 40) perpendicular shocks, and reconnection occurs in the transition region due to Weibel instability. Gingell et al. (2017) demonstrated by hybrid simulations that in the Earth's quasi-parallel bow shock, reconnection occurs in both the transition and downstream regions.

In this letter, we study a quasi-parallel shock by means of two-dimensional (2-D) particle-in-cell (PIC) simulation, using parameters relevant to the Earth's bow shock. We investigate detailed electron and ion kinetic physics in reconnection in shock turbulence, quantifying the reconnection electric field, guide magnetic field, electron and ion flow velocities, and so forth. Our results will be useful for guiding analysis of MMS measurements to investigate reconnection in the Earth's bow shock.

2. 2-D PIC Simulation of Quasi-Parallel Shock and Magnetic Reconnection

2.1. Simulation Setup and Overview of the Shock

The system size is $L_x \times L_y = 375d_i \times 51.2d_i$ (d_i: ion skin depth = 40 simulation grids), the x boundaries are conducting walls, and the y boundaries are periodic. Initially, particles are placed uniformly (with density $n_0 = 100$ superparticles/cell) in uniform fields: magnetic field $\boldsymbol{B} = [B_0 \cos\theta, B_0 \sin\theta, 0]$ (θ: shock angle) and electric field $\boldsymbol{E} = [0,0,E_{z0}]$. A uniform drift speed $\boldsymbol{V_d} = [-V_d,0,0]$ is given to all particles, and $E_{z0} = V_d B_0 \sin\theta/c$. At the left boundary ($x = 0$), particles are forced to be reflected specularly, and a shock wave forms near the boundary, propagating rightward. In the right boundary, new particles are injected [Ohtani & Horiuchi, 2009], and we place a wave damping region in $215d_i \le x \le 375d_i$ to reduce artificial waves due to particle injection (Umeda et al., 2001). The mass ratio $m_i/m_e = 200$, beta values $\beta_i = \beta_e = 1$, and the ratio of the plasma frequency to the electron cyclotron frequency $\omega_{pe}/\Omega_e = 4$. The electron thermal speed $v_{Te} = 14.1v_A$, where v_A is the Alfvén speed in the upstream region. The shock normal angle $\theta = 25°$. We note that there are some limitations in this simulation study: The shock is planar (no curved initial magnetic field), representing only a local region in the Earth's bow shock. Also, the foreshock region is limited within around $200d_i$, and the temporal evolution is less than a few tens of the inverse ion cyclotron frequency, both of which are much smaller than those in an actual fully developed quasi-parallel shock.

Figure 1a shows the magnetic field B_y at $y = 25.6d_i$. The particle drift speed is $V_d = 9v_A$ in the negative x direction, and the shock speed in the simulation frame is $2.4v_A$ in positive x; therefore, the Alfvén Mach number is 11.4, and the shock speed in the shock rest frame $11.4v_A$ is smaller than $v_{Te} = 14.1v_A$, relevant to the Earth's bow shock's condition. In the foreshock, large fluctuations are seen due to instability between the incident and reflected particles [for examples of waves, see Wilson, 2016]. In the ramp, B_y increases rapidly, whose peak is time dependent. At $\Omega_i t = 15.63$, an extended foreshock forms (in $30d_i < x < 60d_i$), and a peak of B_y in the foreshock increases between $\Omega_i t = 15.63$ and 18.75. The foreshock peak eventually becomes comparable to the main peak of the shock, and the new shock front (x~$50d_i$) replaces the old front (x~$30d_i$; shock reformation; Biskamp & Welter, 1972; Lembege & Dawson, 1987; Burgess & Scholer, 2013).

Figures 1b–1d show time evolution of magnetic field lines projected on x-y. In Figure 1b, the shock plane is x~$20d_i$, and there are multiple magnetic islands in the foreshock. During the shock reformation (Figures 1c to 1d), between $\Omega_i t = 15.63$ and 18.75, many islands in the foreshock (x~$30d_i$) at $\Omega_i t = 15.63$ remain there throughout the interval even after the new shock front is formed, and the previous foreshock region became the shock downstream region at $\Omega_i t = 18.75$. After the shock reformation, at $\Omega_i t = 18.75$, islands are newly formed in the new shock front (x~$50d_i$). Ion-scale islands (d_i scale) and electron-scale islands (electron skin depth, d_e scale) coexist in the transition and downstream regions.

Figures 1e–1j display field quantities at $\Omega_i t = 18.75$: electric field E_x (Figure 1e), out-of-plane current density J_z (Figure 1f), out-of-plane magnetic field B_z (Figure 1g), electron density n_e (Figure 1h), and electron fluid velocities V_{ex} (Figure 1i) and V_{ey} (Figure 1j). Color represents each field quantity, and black curves are

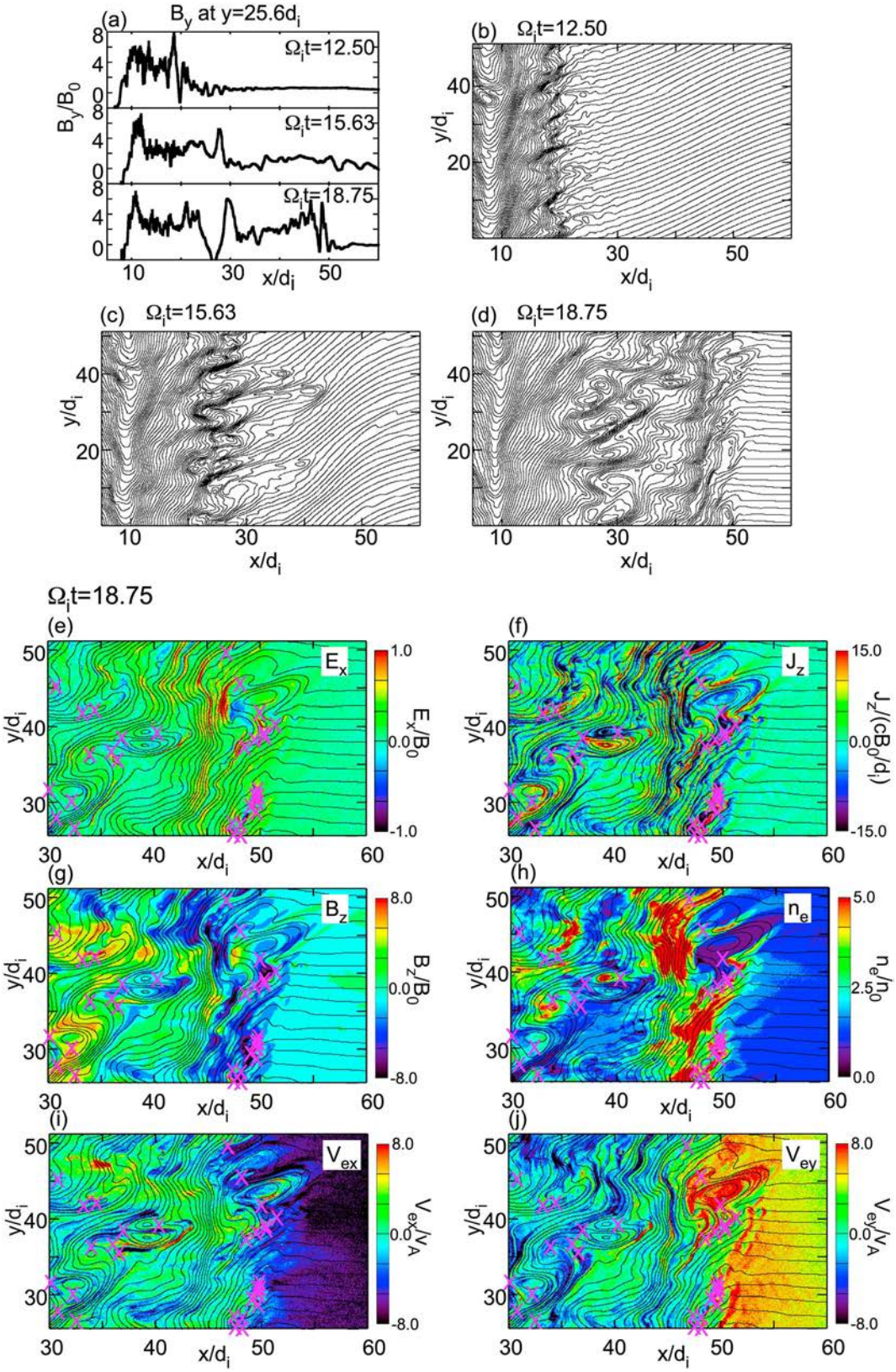

Figure 1. (a) Magnetic field B_y profiles at $y = 25.6d_i$. (b–d) Magnetic field lines in x-y. (e–j) Field quantities at $\Omega_i t = 18.75$. (e) Electric field E_x. (f) Current density J_z. (g) Magnetic field B_z. (h) Electron density n_e. (i, j) Electron fluid velocities V_{ex} and V_{ey}. Black curves denote magnetic field lines. X letters denote X-line positions.

magnetic field lines. The magenta Xs represent reconnection X-line positions. The electric field E_x is basically positive in the transition and downstream regions, and this E_x reflects ions to positive x, while electrons are pulled into the shock.

The current density J_z shows many positive (red) and negative (blue) current sheets in the transition and downstream regions. In the foreshock, there are winding magnetic field lines, and some have antiparallel components in the x-y plane, where reconnection can proceed. The magnetic field B_z in the transition region ($45d_i < x < 50d_i$) becomes negative, because of the decoupling of ion and electron motions (ions are unmagnetized, while electrons are mostly magnetized). The electron motion due to $E_x \times B_y$ pointing toward positive z drags field lines into the positive z direction, resulting in negative B_z. Its magnitude $|B_z|$ is 4–$8B_0$, and reconnection in the transition region becomes guide field reconnection (11 out of 18 X lines in the transition region show negative guide fields $|B_z| > 2B_0$). The guide field strength is the same order as reconnecting magnetic fields.

The electron density (Figure 1h) shows enhancement (more than $5n_0$) in the transition and downstream regions, and the electron fluid velocities (Figures 1i and 1j) show that the transition region with X lines has $V_{ex} < 0$ and $V_{ey} > 0$. The positive V_{ey} is because the magnetic field becomes almost parallel to x in the upstream transition region, and the $E_z \times B_x$ drift points in positive x, even though the far upstream region, $x > 80d_i$ (not shown), still has the field line angle 25° and V_{ey}~0.

2.2. Detailed Reconnection Structures in the Shock Transition Region

Figure 2 shows magnification of a region $47d_i \le x \le 49.5d_i$ and $26.5d_i \le y \le 29d_i$, containing two X lines. Color represents each field quantity, purple curves are magnetic field lines, and white arrows show the electron fluid vector $[V_{ex}, V_{ey}]$ for Figures 2a–2e and the ion fluid vector $[V_{ix}, V_{iy}]$ for Figures 2g–2h.

Let us focus on the right X line at $(x,y) = (48.18d_i, 27.05d_i)$ in Figure 2. Around this X line, there is an almost horizontal positive (red) current sheet (see Figure 2a for J_z), across which B_x changes its sign. The upper region of the current sheet ($y > 27.05d_i$, above the X line) shows $B_x < 0$, while the lower region ($y < 27.05d_i$) shows $B_x > 0$. Above this current sheet, there is a magnetic island. Around the X line, Figures 2d and 2e (V_{ex} and V_{ey}) show bipolar electron jets. Both V_{ex} and V_{ey} show a positive jet in the right side of the X line, and those quantities become negative in the left side. The y thickness of these jets is of the order of $0.1d_i$, which is the electron scale ($d_e = 0.07d_i$). The vector plot (white arrows) shows an inflow from the magnetic island above the current sheet (downward directing white arrows) and a sharp bent of the flow in the upper right side of the X line.

Compared with electrons, ions do not exhibit discernable dynamics in this reconnection region, except for constituting the background flow across the X line. Figures 2g and 2h show ion fluid velocities, and there are no ion jets across the X line. The vector plot (white arrows) shows an almost uniform leftward flow across the X line (with $V_{ix} < 0$). Therefore, this reconnection region is dominantly controlled by the electron physics, similar to the MMS observation by Phan et al. (2018) in the magnetosheath. The island radii in this region are less than $1d_i$, and the separation of each X line/O line is also less than or close to $1d_i$. Our simulation supports the interpretation by Phan et al. (2018), electron-scale reconnection involves only electron dynamics.

Figure 2b shows that around the X line that we are focusing on, the magnetic field $B_z \sim -4B_0$, comparable to the reconnecting B_x in the upper side of the current sheet and twice of the B_x in the lower side. The magnetic field B_z around the X line shows a quadrupolar structure, consistent with laminar reconnection (Ricci et al., 2004): The upper right and the lower left regions of the X line (with respect to the yellow line parallel to the electron jets) have negative $B_z - B_g$, where $B_g = -4B_0$, and the upper left and the lower right regions show positive $B_z - B_g$. These quadrupolar fields are generated due to the electron flow pattern in each quadrant.

Figure 2c shows the energy conversion rate $\boldsymbol{J} \cdot \boldsymbol{E}'$ (where $\boldsymbol{E}' = \boldsymbol{E} + (\boldsymbol{V_e} \times \boldsymbol{B})/c$). When reconnection occurs, $\boldsymbol{J} \cdot \boldsymbol{E}'$ is expected to be positive, indicating energy conversion from fields to particles. Around the X line we are focusing on, $\boldsymbol{J} \cdot \boldsymbol{E}' > 0$.

Figures 2f and 2i show time evolution of field lines, and the X line we are focusing on shows active reconnection, as the island above the X line at $\Omega_i t = 19.0$ contains less magnetic flux contours than $\Omega_i t = 18.75$.

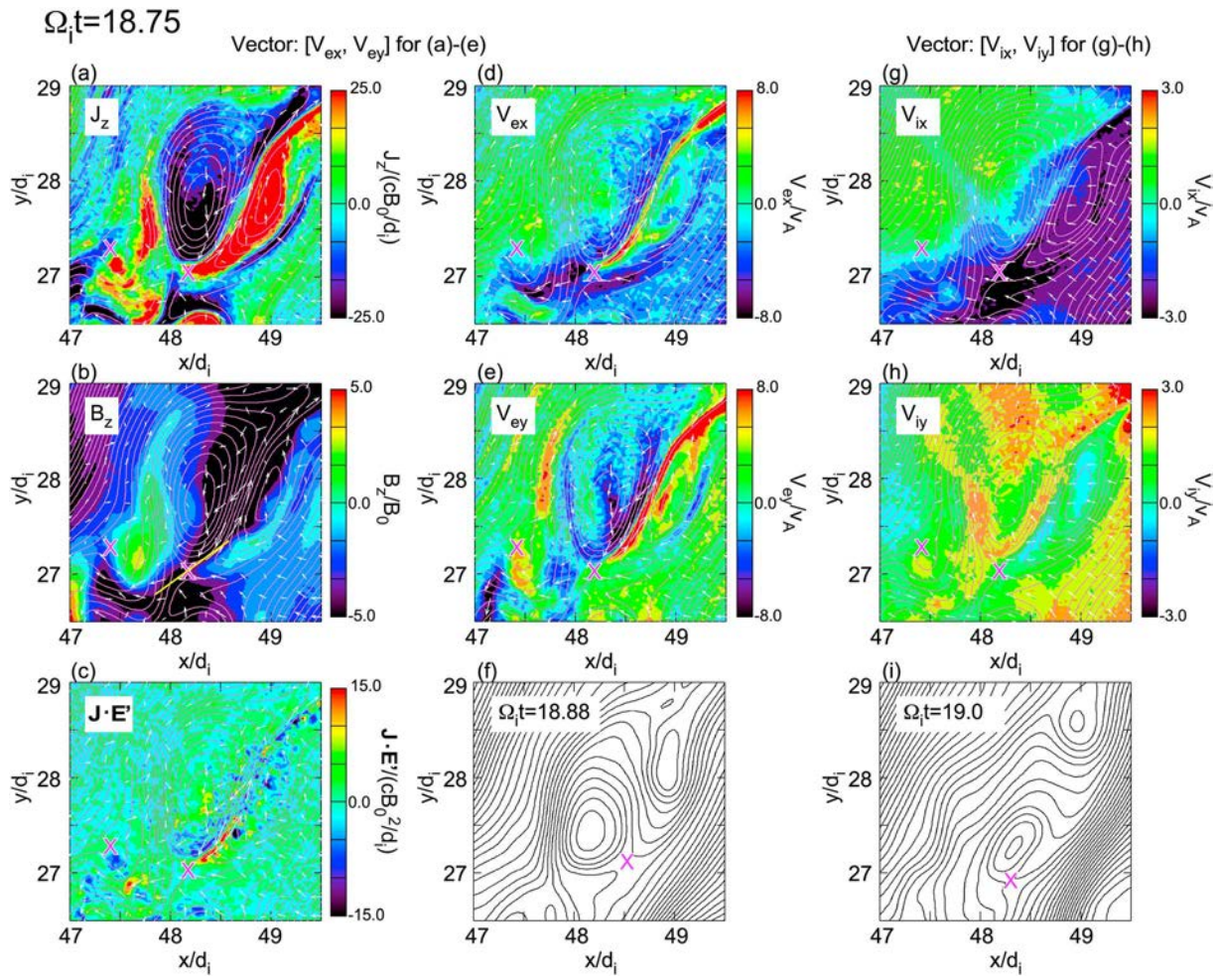

Figure 2. Magnification in $47d_i \le x \le 49.5d_i$ and $26.5d_i \le y \le 29d_i$. (a) Current density J_z. (b) Magnetic field B_z. (c) Energy conversion rate $\boldsymbol{J} \cdot \boldsymbol{E}'$. (d, e) Electron fluid velocities V_{ex} and V_{ey}. (g, h) Ion fluid velocities V_{ix} and V_{iy}. Purple curves denote magnetic field lines. X letters denote X-line positions. White arrows denote vector $[V_{ex}, V_{ey}]$ for (a)–(e) and vector $[V_{ix}, V_{iy}]$ for (g)–(h). (f, i) magnetic field lines at $\Omega_i t = 18.88$ and 19.0.

Figures 3a and 3b show the electron density n_e and the electric field E_z. In the reconnection region we are focusing on (the right X line), n_e is not symmetric across the current sheet, and the upper side (larger y) has smaller density than the lower side (smaller y). The electric field $E_z > 0$ around the reconnection region, and the reconnection electric field averaged around the X line is $E_z = 0.065B_0$. Note that at the X line, the in-plane magnetic field becomes zero, and the reconnection electric field E_z is frame independent.

To compute the normalized reconnection rate, let us investigate the asymmetry in the reconnection region to obtain the theoretical outflow speed (Cassak & Shay, 2007). Figure 3c shows cuts of field quantities across the current sheet, along the vertical black line passing through the X line in Figures 3a and 3b (denoted by 1). The vertical dashed line in Figure 3c represents the X line position, $y = y_X = 27.05d_i$. We measure B_x (reconnecting component, B_1 and B_2 in the two upstream regions) and n_e (n_1 and n_2), to compute $V_{\rm out} = [B_1B_2(B_1+B_2)/(n_1B_2+n_2B_1)]^{1/2}(1/4\pi m_e)^{1/2}$. Here we assume that reconnection is due to only electron; thus, only the electron mass is used. The measured values are $B_1 = 3.23B_0$, $B_2 = 1.26B_0$, $n_1 = 2.92n_0$, and $n_2 = 4.82n_0$. Using these quantities and $m_i/m_e = 200$, we obtain the outflow speed as $V_{\rm out} = 13.7v_{\rm A}$ (where $v_{\rm A}$ is based on B_0, n_0, and m_i).

Let us compare the above theoretical outflow with the simulation data. Since there is a background flow across the X line, let us move to the reference frame where the X line is stationary to measure the outflow speed. During the interval between $\Omega_i t = 18.75$ and $\Omega_i t = 18.77$, the X-line velocity is $[-2.1v_{\rm A}, -2.1v_{\rm A}]$.

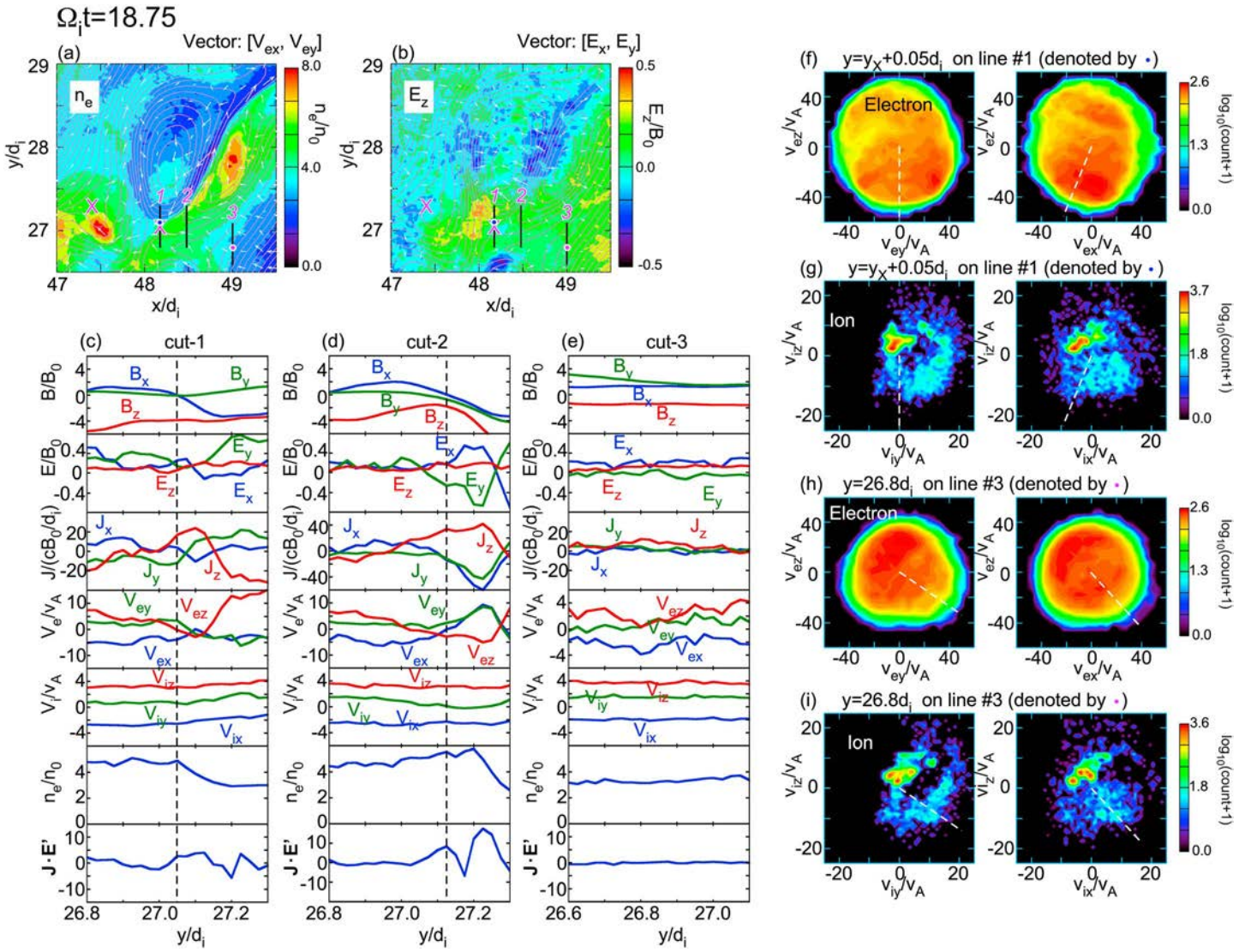

Figure 3. (a) Electron density n_e. White arrows denote vector $[V_{ex}, V_{ey}]$. (b) Electric field E_z. White arrows denote vector $[E_x, E_y]$. (c–e) Field quantities across Vertical Lines 1–3, respectively. (f, g) Reduced electron and ion distribution functions at $y = y_X+0.05d_i$ on Line 1 (y_X: the X-line position). (h, i) Reduced distributions at $y = 26.8d_i$ on Line 3. White dashed lines denote magnetic field direction.

Moving to the X-line stationary frame, we obtained the outflow (in-plane speed $(V_{ex}{}^2+V_{ey}{}^2)^{1/2}$) in the right side of the X line about $18.3v_A$.

Using the theoretical outflow $V_{out} = 13.7v_A$, the reconnection electric field is $E_z = 0.065B_0 = 0.15B_mV_{out}/c$, where B_m is defined as $B_m = (2B_1B_2)/(B_1+B_2) = 1.81B_0$ (Cassak & Shay, 2007). Using the observed outflow $V_{out} = 18.3v_A$, the reconnection electric field becomes $E_z = 0.11B_mV_{out}/c$. Both reconnection rates, 0.15 and 0.11, indicate fast reconnection.

The second cut (line 2 in Figures 3a and 3b) is located $0.25d_i$ away in positive x from the X line, passing through near the highest electron outflow. The vertical dashed line in Figure 3d is the B_x reversal. Along this cut, V_{ex} changes from negative to positive, and V_{ey} enhances from almost zero to positive. The current density J_z peaks near the V_{ex} and V_{ey} peaks. The energy conversion rate $\boldsymbol{J}\cdot\boldsymbol{E}'$ becomes strongly enhanced in the V_{ex} and V_{ey} jets.

Electron distribution functions show acceleration due to reconnection. Figures 3f and 3g show reduced distributions (integrated along the out-of-plane component in each velocity plane) on line 1, at $y = y_X$

$+0.05d_i = 27.1d_i$, slightly away from the X line (at the peak of J_z). The left and the right panels show the distributions in v_{ey}-v_{ez} and v_{ex}-v_{ez}, respectively, and dashed white lines represent the direction of magnetic field. The electron distribution (Figure 3f) shows that there are many electrons whose $v_{ez} < 0$, accelerated by $E_z > 0$, along the guide field direction. The ion distribution (Figure 3g) shows cold incident ions (the red blob near $v_{iz} = 5v_A$) and hot ions reflected by the shock (green component surrounding the cold ions). Figures 3h and 3i show distributions on line 3 (cuts are shown in Figure 3e), at $x = 49d_i$ and $y = 26.8d_i$, which is in the upstream region of this reconnection site. The electron distribution (Figure 3h) is cooler than the distribution (Figure 3f), and many electrons show positive v_{ez}, consistent with the fluid velocity $V_{ez} > 0$ in Figure 3e. Comparing Figure 3f (reconnection region) and Figure 3h (upstream region), the highest parallel speed (parallel to the magnetic field) in Figure 3f is higher than the highest parallel speed (antiparallel to the magnetic field) in Figure 3h. We conclude that the accelerated electrons ($v_{ez} < 0$) in Figure 3f are due to the reconnection electric field $E_z > 0$. While electrons are accelerated due to reconnection, the ion distribution (Figure 3g) is similar to the distribution (Figure 3i), and we conclude that ions do not respond to the reconnection there.

When a magnetic island's size is several times d_i, ion physics becomes important in reconnection sites. Figures 4a and 4b show time evolution of field lines (black curves) and the ion fluid velocity V_{iy} from $\Omega_i t = 17.97$ to 18.75. In the transition region, there are streaks of large positive V_{iy} (red regions), each of which involves multiple X lines. In the large V_{iy} regions with multiple X lines, the separation between the X lines is the electron scale (several d_e). In those strong V_{iy} regions (ion jets), V_{iy} exceeds $10v_A$, larger than the local Alfvén speed based on reconnecting magnetic fields and density. Only ion jets with positive V_{iy} are seen, and there are no negative V_{iy} jets.

Figures 4c and 4d show magnification of the ion-scale island around $x = 50d_i$ and $y = 44d_i$ at $\Omega_i t = 18.75$. The vector arrows are for $[V_{ix}, V_{iy}]$ and $[V_{ex}, V_{ey}]$, respectively. There are five X lines below the magnetic island region (blue and magenta Xs). The ion fluid (Figure 4c) shows a y-directional flow across the island, and this jet comes from reconnection regions below this region (magenta X lines), covering the X line right below the magnetic island (blue X line at $x = 49.9d_i$ and $y = 41.8d_i$), which we will focus on for the analysis of the reconnection structure associated with this magnetic island. The ion jet thickness is a few d_i. In contrast, Figure 4d shows electron jets with $V_{ey} > 0$ from a few X lines below the magnetic island, and they exceed the ion jet speed. The electron jet thicknesses are the electron scale. Both ion and electron flows are super-Alfvénic (speeds more than $10v_A$).

Figures 4g and 4h show cuts of field quantities along the horizontal black lines in Figures 4c and 4d, #4 and #5, at $y = 41.825d_i$ and $y = 42.5d_i$, respectively. Line 4 crosses the blue X line we are focusing on, and the magnetic field B_y reverses its sign at $y = 49.9d_i$ (vertical dashed line), and B_y near the current sheet edges (see the negative J_z peak in the third panel) is around $1.2B_0$ in the left and $-3.7B_0$ in the right. The guide field is $B_z = -2.4B_0$ at the X line, the same order of B_y. The electric field E_z averaged around the X line (reconnection electric field) is $E_z = -0.027B_0$. The ion velocity V_{iy}~$10v_A$, while electron velocity V_{ey} has a peak ($12.7v_A$) in the right side of the X line. The fast ion flow ($10v_A$) is not the result of the reconnection at the blue X line but due to another physics (either reconnection or instability around the magenta X lines near $y = 38d_i$. Detailed physics is beyond the scope of the paper). The density n_e is almost flat across the current sheet. The energy conversion rate $\boldsymbol{J} \cdot \boldsymbol{E}' > 0$ in the current sheet (negative J_z).

Field quantities on Line 5 (Figure 4h), which is about $0.7d_i$ away from Line 4, show variations similar to Figure 4g, but the flow speeds in the right side of the B_y reversal (vertical dashed line), $x > 49.65d_i$, show noticeable differences from Figure 4g. Both peaks of V_{ex} and V_{ey} in the right side of the B_y reversal becomes larger in Figure 4h than those in Figure 4g. Also, for ions, the large V_{iy} region (~$9v_A$) is extended to the right side of the B_y reversal in Figure 4h, and V_{ix} in $x > 49.65d_i$ reaches positive in Figure 4h, compared with negative V_{ix} in the right side of the X line in Figure 4g. These enhancements of the fluid velocities are due to reconnection at the X line right below the magnetic island (blue X line).

Since there are large flows near the X line right below the island, let us move to the X-line stationary frame to discuss the outflows, using the X-line velocity $[-4.9v_A, 2.8v_A]$. Figures 4e and 4f show the in-plane flows, $\mathrm{sgn}(V_{jx})|V_{j-xy}|$, where $j = i$ or e, and $|V_{j-xy}| = (V_{jx}^2 + V_{jy}^2)^{1/2}$ in the X-line stationary frame. In this frame, both ions and electrons flow into the X line from the lower left side, and they are ejected to the upper right

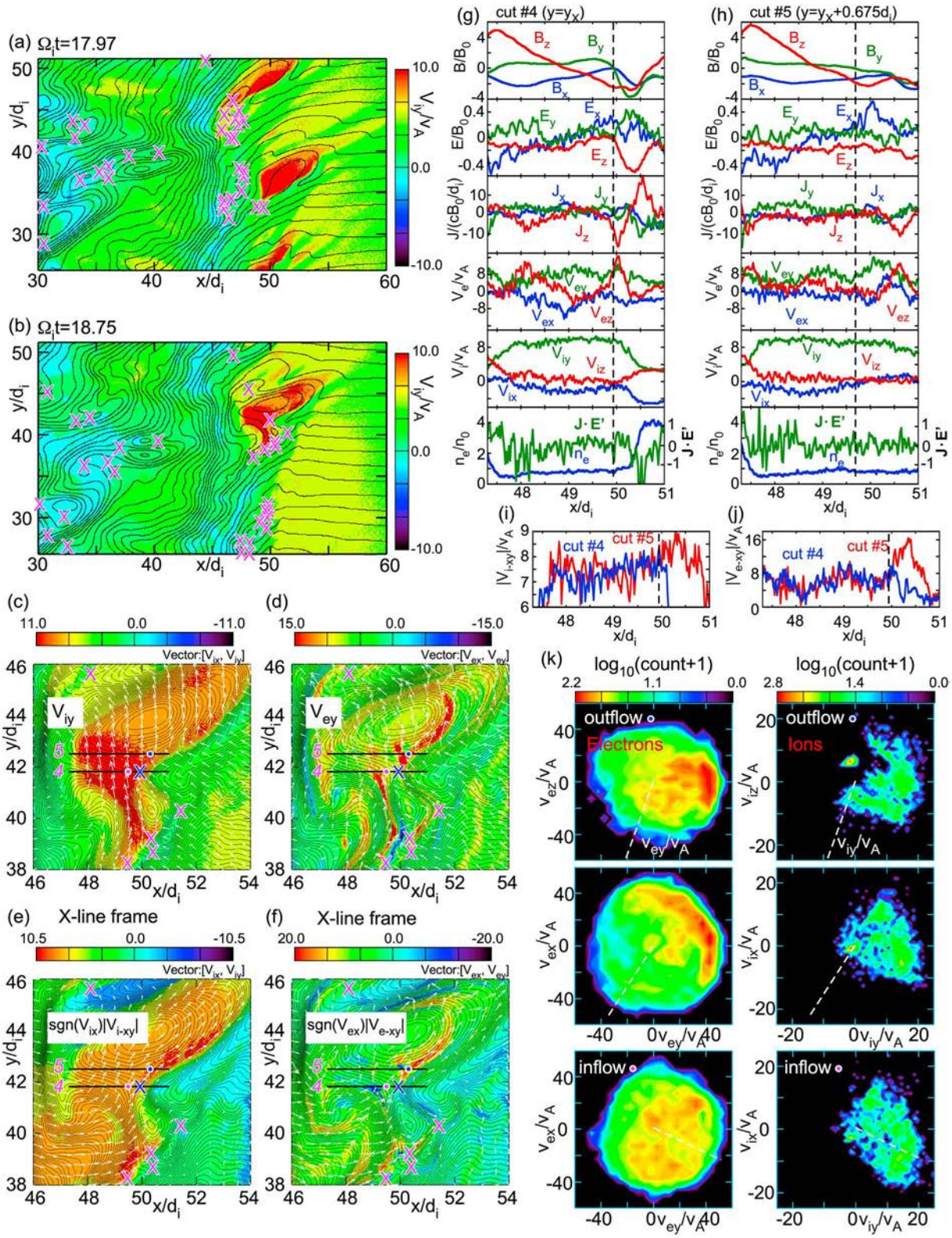

Figure 4. (a, b) Ion fluid velocity V_{iy} at $\Omega_i t$ = 17.97 and 18.75. (c, d) Magnification of an ion-scale island at $\Omega_i t$ = 18.75. (e, f) In-plane flow speeds in the X-line stationary frame. (g, h) Field quantities along the black Lines 4 and 5 in (c) and (d). (i, j) In-plane speed in the X-line stationary frame. (k) Reduced electron (left) and ion (right) distributions in the outflow and inflow regions (at blue dot and magenta dot, respectively). White dashed lines denote magnetic field direction.

side, where the flow speeds become larger than those in the inflow regions (the lower left side of the X line). Figures 4i and 4j show the cuts of $|V_{j-xy}|$ in Lines 4 (blue) and 5 (red). The outflow speed increase (compared with the speed at the X line) for ion is around $1V_A$ and that for electron is around $7V_A$. These increases are due to reconnection.

The occurrence of reconnection in a fast background flow was studied by Liu and Hesse (2016), where only a one-sided jet was observed. The situation in this ion-scale island is similar to that study, but further studies are required for details.

The reconnection electric field normalized with $B_m V_{out}/c$ is 0.081, where $B_m = (2B_1B_2)/(B_1+B_2) = 1.82B_0$ (with $B_1 = 1.21B_0$ and $B_2 = 3.68B_0$) and V_{out} is the ion outflow speed $|V_{i-xy}|$ in the X-line stationary frame $10.3v_A$. Using the formula by Cassak and Shay (2007), the outflow speed is predicted as $V_{out} = [B_1B_2(B_1+B_2)/(n_1B_2+n_2B_1)]^{1/2}(1/4\pi m_i)^{1/2} = 2.18v_A$ (with $n_1 = 0.87n_0$ and $n_2 = 1.12n_0$), but the observed ion jet speed ($10v_A$) is almost five times larger, because of the background flow structure. We note that some X-line regions show spatially fluctuating E_z patterns because of waves in turbulent plasma, and determining the reconnection rates requires further studies.

Figure 4k shows distribution functions in the outflow region, at $x = 50.3d_i$ on Line 5 (top and middle panels), near the electron jet (blue dot in Figures 4c–4f) and distributions in the inflow region, at $x = 49.5d_i$ on Line 4 (magenta dot in Figures 4c–4f). These distributions are in the simulation frame. Electrons in the outflow (top and middle distributions) are accelerated in $v_{ey} > 0$ and $v_{ex} > 0$, compared with the distribution in the inflow (bottom). The ion distribution in v_{iy}-v_{iz} (top right) shows a similarity to Figures 3g and 3i (a core + ions reflected by the shock), and the distribution in v_{iy}-v_{ix} (middle right) shows that some reflected ions (a yellow blob in $v_{iy} > 0$ and $v_{ix} < 0$) are shifted to the positive v_{ix} direction, compared with the inflow ions (bottom right). This shift of v_{ix} causes the ion outflow formation in the X-line stationary frame.

Some accelerated particles (in Figure 4k as well as in Figure 3f) are moving faster than the fluid velocities, and once they are ejected from reconnection sites, they may be injected into other acceleration mechanisms in the shock.

3. Conclusion

We have investigated a quasi-parallel shock (shock angle 25°) by a 2-D local PIC simulation and demonstrated reconnection in shock turbulence. Current sheets form in the transition and downstream regions, and ion-scale and electron-scale magnetic islands coexist. In the transition region, the out-of-plane magnetic field is generated due to the Hall effect, and guide field reconnection occurs. In electron-scale island regions, reconnection with only electron jets has been identified, whose thickness is of the order of a few d_e. Ions constitute background flows in those regions. A reconnection rate 0.1–0.2 is observed, based on the asymmetric reconnection model with only electron physics. The quadrupolar out-of-plane magnetic field forms due to electron flows. In ion-scale island regions, reconnection involves both ions and electrons, in super-Alfvénic flows in the shock. The ion jet thickness is a few d_i, and the reconnection rate around 0.1 is observed. In those electron-scale and ion-scale island regions, distribution functions show acceleration signatures due to the reconnection electric field.

Acknowledgments
The work was supported by DOE Grant DESC0016278, NSF Grants AGS-1619584 and AGS-1552142, NASA Grant 80NSSC18K1369, and the NASA MMS project. The work was partially supported by the International Space Science Institute's (ISSI) International Teams programme. Work at the University of Bergen was supported by the Research Council of Norway/CoE under Contract 223252/F50. PIC simulations were performed on Pleiades at the NASA Advanced Supercomputing, and subsets of simulation data are available from The Digital Repository at the University of Maryland (DRUM; http://hdl.handle.net/1903/21807).

References

Biskamp, D., & Welter, H. (1972). Numerical studies of magnetosonic collisionless shock waves. *Nuclear Fusion*, *12*(6), 663–666. https://doi.org/10.1088/0029-5515/12/6/006

Bohdan, A., Niemiec, J., Kobzar, O., & Pohl, M. (2017). Electron pre-acceleration at nonrelativistic high-Mach-number perpendicular shocks. *Astrophysical Journal*, *847*(1), 71. https://doi.org/10.3847/1538-4357/aa872a

Burgess, D., Möbius, E., & Scholer, M. (2012). Ion acceleration at the Earth's bow shock. *Space Science Reviews*, *173*(1-4), 5–47. https://doi.org/10.1007/s11214-012-9901-5

Burgess, D., & Scholer, M. (2013). Microphysics of quasi-parallel shocks in collisionless plasmas. *Space Science Reviews*, *178*(2-4), 513–533. https://doi.org/10.1007/s11214-013-9969-6

Cassak, P. A., & Shay, M. A. (2007). Scaling of asymmetric magnetic reconnection: General theory and collisional simulations. *Physics of Plasmas*, *14*(10), 102114. https://doi.org/10.1063/1.2795630

Gingell, I., Schwartz, S. J., Burgess, D., Johlander, A., Russell, C. T., Burch, J. L., et al. (2017). MMS observations and hybrid simulations of surface ripples at a marginally quasi-parallel shock. *Journal of Geophysical Research: Space Physics*, *122*, 11003. https://doi.org/10.1002/2017JA024538

Gingell, I., Schwartz, S. J., Eastwood, J. P., Burch, J. L., Ergun, R. E., Fuselier, S., et al. (2019). Observations of magnetic reconnection in the transition region of quasi-parallel shocks. *Geophysical Research Letters*, *46*, 1177–1184. https://doi.org/10.1029/2018GL081804

Karimabadi, H., Roytershteyn, V., Vu, H. X., Omelchenko, Y. A., Scudder, J., Daughton, W., et al. (2014). The link between shocks, turbulence, and magnetic reconnection in collisionless plasmas. *Physics of Plasmas*, *21*(6), 062308. https://doi.org/10.1063/1.4882875

Lembege, B., & Dawson, J. M. (1987). Self-consistent study of a perpendicular collisionless and nonresistive shock. *The Physics of Fluids*, *30*(6), 1767–1788. https://doi.org/10.1063/1.866191

Liu, Y.-H., & Hesse, M. (2016). Suppression of collisionless magnetic reconnection in asymmetric current sheets. *Physics of Plasmas*, *23*(6), 060704. https://doi.org/10.1063/1.4954818

Matsumoto, Y., Amano, T., Kato, T. N., & Hoshino, M. (2015). Stochastic electron acceleration during spontaneous turbulent reconnection in a strong shock wave. *Science*, *347*(6225), 974–978. https://doi.org/10.1126/science.1260168

Ohtani, H., & Horiuchi, R. (2009). Open boundary condition for particle simulation in magnetic reconnection research. *Plasma and Fusion Research*, *4*, 024. https://doi.org/10.1585/pfr.4.024

Phan, T. D., Eastwood, J. P., Shay, M. A., Drake, J. F., Sonnerup, B. U. Ö., Fujimoto, M., et al. (2018). Electron magnetic reconnection without ion coupling in Earth's turbulent magnetosheath. *Nature*, *557*(7704), 202–206. https://doi.org/10.1038/s41586-018-0091-5

Retinò, A., Sundkvist, D., Vaivads, A., Mozer, F., André, M., & Owen, C. J. (2007). In situ evidence of magnetic reconnection in turbulent plasma. *Nature Physics*, **3**, 235.

Ricci, P., Brackbill, J. U., Daughton, W., & Lapenta, G. (2004). Collisionless magnetic reconnection in the presence of a guide field. *Physics of Plasmas*, *11*(8), 4102–4114. https://doi.org/10.1063/1.1768552

Scholer, M. (1993). Upstream waves, shocklets, short large-amplitude magnetic structures and the cyclic behavior of oblique quasi-parallel collisionless shocks. *Journal of Geophysical Research*, *98*(A1), 47–57. https://doi.org/10.1029/92JA01875

Scholer, M., Kucharek, H., & Jayanti, V. (1997). Waves and turbulence in high Mach number nearly parallel collisionless shocks. *Journal of Geophysical Research Space Physics*, *102*, 9821–9833. https://doi.org/10.1029/97ja00345

Umeda, T., Omura, Y., & Matsumoto, H. (2001). An improved masking method for absorbing boundaries in electromagnetic particle simulations. *Computer Physics Communications*, *137*(2), 286–299. https://doi.org/10.1016/S0010-4655(01)00182-5

Vörös, Z., Yordanova, E., Varsani, A., Genestreti, K. J., Khotyaintsev, Y. V., Li, W., et al. (2017). MMS observation of magnetic reconnection in the turbulent magnetosheath. *Journal of Geophysical Research: Space Physics*, *122*, 11,442–11,467. https://doi.org/10.1002/2017ja024535

Wang, S., Chen, L. J., Bessho, N., Hesse, M., Wilson, L. B. III, Giles, B., et al. (2019). Observational evidence of magnetic reconnection in the terrestrial bow shock transition region. *Geophysical Research Letters*, *46*, 562.

Wilson, L. B. III (2016). Low frequency waves at and upstream of collisionless shocks. In A. Keiling, D.-H. Lee, & V. Nakariakov (Eds.), *Low-frequency waves in space plasmas, Geophysical Monograph Series*, (Vol. 216, pp. 269–291). Washington, DC: American Geophysical Union. https://doi.org/10.1002/9781119055006.ch16

Wu, C. S. (1982). Physical mechanisms for turbulent dissipation in collisionless shock waves. *Space Science Reviews*, *32*, 83.

Yordanova, E., Vörös, Z., Varsani, A., Graham, D. B., Norgren, C., Khotyaintsev, Y. V., et al. (2016). Electron scale structures and magnetic reconnection signatures in the turbulent magnetosheath. *Geophysical Research Letters*, *43*, 5969–5978. https://doi.org/10.1002/2016GL069191